Supplement of Biogeosciences, 12, 1683–1696, 2015
http://www.biogeosciences.net/12/1683/2015/
doi:10.5194/bg-12-1683-2015-supplement

Biogeosciences Open Access

Supplement of

Tidal controls on trace gas dynamics in a seagrass meadow of the Ria Formosa lagoon (southern Portugal)

E. Bahlmann et al.

Correspondence to: E. Bahlmann (enno.bahlmann@zmaw.de)

Supplementary Material

Enno Bahlmann, Richard Seifert, University of Hamburg, Institute for Biogeochemistry and Marine Chemistry, Bundesstraße 55, 20146 Hamburg, Germany

Operation Principle of the flux chamber

Flux chambers have been widely applied to study trace gases in terrestrial systems (Gao et al., 1997; Gao and Yates, 1998; Kim and Lindberg, 1995; Zhang et al., 2002; Pape et al., 2009) and in coastal intertidal systems (Van der Nat and Middelburg, 2000). Flux chambers inevitably alter the physical and chemical conditions at the enclosed surface and thus may affect the trace gas fluxes. Under aerial conditions, problems may arise from pertubations of the turbulent fields at the interface, introduction of artificial gradients, pertubations of the thermal environment and the gas composition inside the chamber (Gao et al., 1997; Meixner et al., 1997; Gao & Yates, 1998; Zhang et al., 2002; Pape et al., 2009). Under submersed conditions solid static chambers will most likely introduce stagnant conditions and thus reduce the diffusive exchange and suppress advective exchange (Cook et al., 2007). This has for instance been shown for oxygen (Billerbeck et al., 2006; Werner et al., 2006; Kim & Kim, 2007; Cook et al., 2007; Jansen et al, 2009), total inorganic carbon (Cook et al., 2007) and dissolved organic matter (Huettel et al., 1996). Tengberg et al. (2004) compared three different types of stirred benthic chambers and found no significant differences between these chambers. The authors concluded that benthic chambers are insensitive to the hydrodynamic conditions as long as the water is well mixed and the sediment is not re-suspended.

The trace gas fluxes and their sensitivity against alterations of the aerodynamic and hydrodynamic conditions at the interface further depend on the nature of the source or sink. In particular deposition fluxes of reactive trace gases, which are dependent on the headspace concentration inside the chamber, are very sensitive towards the aerodynamic properties of the chamber (Meixner et al., 1997; Pape et al., 2009). This also holds true for emissions having a constant and uniform source (e.g. compounds whose concentration in the soil or sediment are controlled by a rapid chemical equilibrium) (Gao & Yates, 1987). This has for instance been shown for mercury (Zhang et al., 2002).

It has been suggested that the emission fluxes of most VOCs are insensitive against the turbulent conditions inside the chamber, because their production is independent of the

headspace concentration (Pape et al., 2009). Anyhow, as the nature of the source/sink is often poorly constrained, it is good practice to minimize the disturbance of the aerodynamic conditions. Here we provide a description of the laboratory performance tests of our chamber system under aerial und submersed condition.

The flux of an inert trace gas above an enclosed surface is determined by the mass balance of the chamber (e.g. Gao & Yates 1998; Zhang et al., 2001; Pape et al., 2009):

$$\frac{dN(t)}{dt} = V\frac{c_{out}}{dt} = A \times F_c + Q(c_{out} - c_{in}) \quad (1)$$

Where N is the absolute molar mass of a trace gas inside the chamber, V is the volume of the chamber [L^{-3}], c_{out} and c_{in} are the molar densities of the target compounds [N L^{-3}] at the outlet and the inlet of the flux chamber, F_c is the interfacial flux [N L^{-2} t^{-1}] above the enclosed surface A [L^2] and Q_N is the flushing flow rate of dry air through the chamber [L^3 t^{-1}, at 1013.25 mbar and 298.15 K]. N, L, and t are dimensions of moles, length, and time, respectively. A basic assumption within this mass balance is that the chamber is well mixed and thus the headspace concentration inside the chamber can be reasonably well be approximated from the outlet concentration. For a dynamic chamber in steady state the time derivative becomes zero Pape et al., 2009). Accordingly, net fluxes above the covered surface can be calculated from the concentration difference between the outlet and inlet of the chamber:

$$F_c = \frac{Q_n}{A}\,(c_{out} - c_{in}) \quad (2)$$

The physical nature of trace gas fluxes across natural interfaces is commonly described in terms of a multiresistance model (Hicks et al, 1987). This model has been applied to flux chambers (Gao et al., 1997; Zhang et al., 2002; Pape et al., 2009) and is applicable for studies under aerial as well as submersed conditions:

$$F_i = \left(c_s - c_{ag}\right) \times h_i = \frac{c_s - c_a}{R_i} \quad (3)$$

Where F_i denotes the flux across the interface, c_s is the concentration in the substrate (e.g. the sediment or the seagrass leaf), c_g is the gas concentration on the air side of the interface h_i [L t^{-1}] is the overall exchange coefficient and R_i [t L^{-1}], the reciprocal of h_i, is the overall transport resistance. The overall transfer resistance is given by the sum of the aerodynamic or

hydrodynamic resistance (R_a), the resistance of the quasi laminar boundary layer above the sediment (R_b) and the diffusive resistance of the substrate (R_s):

$$R_i = R_a + R_b + R_s = R_c + R_s \quad (4)$$

R_a and R_b can be combined to R_c representing the overall aerodynamic transfer resistance of the chamber (Zhang et al., 2002). While R_c depends on the aerodynamic properties of the chamber, R_s depends on the sediment properties. The sensitivity of the overall flux against the aerodynamic properties depends on the magnitude R_c and R_s. When both share the same magnitude the flux across the interface depends on R_c and R_s. On the other hand, when R_s becomes large relative to R_c the flux is mainly governed by R_s and the aerodynamic properties of the chamber have a negligible effect on the trace gas fluxes (Zhang et al. 2002).

Aerial conditions

A pressure deficit inside the chamber may cause an artificial advective exchange (Gao & Yates, 1987). In this setup air is pumped through the chamber resulting in a slight overpressure. From Hagen Poiseilles law we calculated an overpressure of 0.8 Pa for a flushing flow rate of 3 L min^{-1}. Thus we exclude any artificial advective exchange for aerial conditions.

A basic assumption of dynamic flux chamber measurements is that the chamber is in steady state, meaning that the time averaged net flux calculated from the inlet and outlet concentrations equals the time averaged net flux across the interface of interest. A convenient measure for the time required to establish steady state conditions is the response time (t_r) of the chamber denoting the time after disturbance (such as a sudden change in emission) required to achieve 37% (e^{-1}x 100) of the initial perturbation. Provided that the change after a perturbation is exponential, 95% of steady state will be reached after three times the response time. Under aerial conditions the response time can be estimated from the flushing flow rate and the chamber volume and is given by

$$t_r = \frac{V}{Q} \quad (5)$$

At a typical flushing flow rate of 3 L min^{-1} the response time of our chamber system is 2 minutes. Pre-tests revealed that complete mixing of the chamber volume is achieved within 0.4 min. Both are in the mid-range of reported time scales (Pape et al., 2009) Hence, with

respect to our sampling frequency, we can safely assume complete mixing of the air inside the chamber.

To determine R_c for our flux chamber we have measured the CO_2 flux above 1N NaOH. 4 L of 1N NaOH were carefully filled into a 10L Duran glass bottle avoiding wetting of the bottle walls and leaving a headspace of 6L being comparable to the headspace of the field chamber. The NaOH solution was gently stirred (50 RPM). Ambient air (407±3 ppm CO_2) was pumped through the chamber at flushing flow rates between 0.5 and 5 L min^{-1} and the concentration was measured at the outlet of the chamber. Under the assumption that the NaOH solution provides a perfect sink for CO_2, R_s becomes negligible and R_c can be estimated according to:

$$R_c = \frac{-c_{out}}{c_{out}-c_{in}} \times \frac{A}{Q} \quad (6)$$

For flushing flow rates from 0.5 to 4 L min^{-1} the uptake flux increased logarithmically from 16.4 to 57.4 mmol $m^2 h^{-1}$ ($F = 19.224*\ln(Q) + 29.697$; $R^2 = 0.9967$) and remained on this level at an increased flow rate of 5 L min^{-1}. Surprisingly, R_c increased with increasing flushing flow rate from 0.162 h m^{-1} (Q = 0.5 L min^{-1}) to 0.206 h m^{-1} at Q = 5.0 L min^{-1}. We attribute this increase to an insufficient renewal of the liquid surface film limiting the CO_2 uptake at high CO_2 loads. However, these results provide an upper estimate of 0.162 hm^{-1} for R_c at a flushing flow rate of 3.0 L min^{-1}. The sediment side transfer resistance is commonly computed from the diffusivity of the sediment surface layer and its thickness (Gao et al., 1997; Zhang et al., 2002).

$$R_s = \frac{l}{0.6 D_0 p_s} \quad (7)$$

Where l [L] denotes the thickness of the sediment surface layer, 0.6 is an empirical scaling factor accounting for the tortuosity of the pores (Penman 1940 a, b), D_0 [$L^2 t^{-1}$] is the diffusion coefficient in air and p_s is the fraction of the air filled pore space. Following Zhang et al. (2002) we used a thickness of 0.005 m to estimate R_s. With $D_0(CO_2)$ = 0.054 $m^2 h^{-1}$ and p_s ranging from 0.01 to 0.1 for water logged intertidal sediments R_s is estimated to range from 1.54 to 15.4 h m^{-1} being about one to two orders of magnitude larger than Ra. Given this it is reasonable to assume that the trace gas flux across the sediment surface is mainly governed by the sediment resistance. Our tests further suggest a minor effect of the flushing flow rate on the atmospheric transfer resistance making the overall transfer resistance insensitive against the aerodynamic properties of the chamber.

The same principles apply to the trace gas exchange across the sea grass leafs. In contrast to higher plants on land, seagrass lacks any stomata and gas transport is facilitated across the thin cuticula of the leaves. MacFarlane (1992) reports a CO_2 permeability of 2.1 µm s^{-1} for the cuticula of submersed plants. This corresponds to a transfer resistance of 132 h m^{-1}. Using a leaf area index of 3 - 5 for Z. noltii in the Ria Formosa (Pérez-Lloréns & Niell, 1993) we can normalize the transfer resistance to the enclosed surface area and estimate its range to 26.5 to 46 h m^{-1}. In summary we can safely assume that during air exposure the gas exchange across the sediment surface and the seagrass leafs is not dependent on the aerodynamic properties of the chamber.

The measured trace gas fluxes may be affected by the enclosure effect (i.e. the deviation of the trace gas concentration in the chamber from ambient concentrations above the ground). The effect of the flushing flow rate depends on the overall transfer resistance. When assuming a constant and uniform source (or sink) the effect of the flushing flow rate under steady state conditions is given by (eq. 22. in Zhang et al., 2002):

$$F_{steady} = \frac{c_s - c_i}{R_i} \times \frac{1}{1+\frac{A}{R_i \times Q}} \quad (8)$$

Thus the enclosure effect is given by:

$$\frac{F_{steady}}{F_{limQ\to\infty}} = \frac{1}{1+\frac{A}{R_i \times Q}} \quad (9)$$

With a bottom surface area of 0.037 m² and an overall transfer resistance ranging from 1.62 to 15.6 h m^{-1} the steady state flux at a flushing flow rate of 3 L min^{-1} [0.18 m^3 h^{-1}) resembles more than 96% of the maximum flux ($F_{limQ\to\infty}$) suggesting a negligible effect of the flushing flow rate on the trace gas exchange. This is also supported by the CO_2 uptake above 1N NaOH.

During submersion

Our field data clearly show that during submersion the sediment/water flux is governed by advective transport. A treatment of these processes is beyond the scope of this paper as it would require detailed hydrodynamic data of the chamber system and of the surface. Furthermore, Tengberg et al. (2004) suggested benthic chambers being insensitive to the hydrodynamic conditions as long as the water is well mixed and the sediment is not re-

suspended. Re-suspension of the sediments was avoided during the experiments and has been checked visibly. The gas flow through the chamber introduced a water flow in the order of 10 to 15 cm s^{-1} providing a corresponding boundary layer thickness in the range of 60 to 120 µm where the carbon uptake is mainly enzymatically limited. The visible inferred mixing time was in 1.1 min. We therefore limit the discussion of the chamber performance under submersed conditions to the gas exchange and the response time of the chamber.

During submersion the sediment and the benthic vegetation exchange the trace gases with the water phase. The dissolved trace gases are equilibrated with ambient air. As a consequence the trace gas concentration inside the chamber is not represented by the outlet concentration any more. Further dissolved trace gases are exchanged with the surrounding water through the U-tube connecting the chamber with the surrounding water. Thus we have to modify the mass balance of the chamber for submersed conditions:

$$\frac{dN(t)}{dt} = V\frac{c_{wk}}{dt} = A \times F_c + F_w + Q(c_{out} - c_{in}) \qquad (10)$$

where c_{wk} is the concentration of the dissolved trace gases inside the chamber and F_w accounts the exchange of dissolved trace gases with the surrounding water via the U-tube. Under submersed conditions, F_c will depend on the volatility of the trace gas (given by the dimensionless Henrys law constant) and the water air transfer resistance of the chamber system. In analogy to the air sea gas exchange the flux at the chamber outlet can be computed as:

$$Q(c_{out} - c_{in}) = k_{aw} \times (c_w/H - c_{in}) = \frac{(c_w/H - c_{in})}{R_{aw}} \qquad (11)$$

where k_{aw} is the gas exchange velocity [L t^{-1}] depending on the flushing flow rate (Q) and the chamber design (in particular the chamber geometry and the gas bubble geometry), R_{aw} = $1/k_{aw}$ is the corresponding transfer resistance, c_w is the water concentration [N L^{-3}] and c_{in} the inlet concentration represents ambient concentrations. F_w can be calculated according to:

$$F_w = \frac{(c_{wk} - c_{wa})}{R_{wex}} \qquad (12)$$

Here Δc_w denotes the concentration difference between the chamber and the surrounding water and R_{wex} is the transfer resistance of the water exchange. Insertion of eq. 11 and 12 in eq. 10 leads to:

$$\frac{dN(t)}{dt} = V\frac{c_{wk}}{dt} = A \times F_c + \frac{(c_{wk} - c_{wa})}{R_{wex}} + \frac{(c_w/H - c_{in})}{R_{aw}} \quad (13)$$

R_{aw} was derived from the slope of the concentration at the outlet of the chamber after injecting seawater enriched in methane and CO_2 into the chamber. Under the experimental conditions $A \times F_c + \frac{(c_{wk} - c_{wa})}{R_{wex}}$ is zero and the change in the dissolved trace gases is given by:

$$\frac{c_{wk}}{dt} = \frac{c_{wk} - c_{in} \times H}{V \times H \times R_{aw}} \quad (14)$$

Thus the response time can be calculated from:

$$c_{wk(t)} = (c_{wk(0)} - c_{in} \times H) \times e^{-\frac{t}{V \times H \times R_{aw}}} \quad (15)$$

CH_4

For methane R_{aw} of the submersed chamber was derived from the slope of concentration over time at the outlet of the chamber after injection of seawater enriched in methane. Artificial seawater with 35 PSU was prepared from commercially available sea salt for the tests with the pH adjusted to 8.1±0.1. The chamber was continuously purged with synthetic air (Westfalen, Germany) having a CH_4 concentration below the detection limit. For all experiments the flow was set to 3.0 L min^{-1}. Prior the experiment the chamber was flushed with synthetic air for 1h to remove traces of CH_4. 250 ml of seawater were withdrawn from the chamber and were equilibrated with methane (30% in synthetic air.) 24h at 1.3 bar and 4°C. These solutions were injected into the chamber and the decline of the methane concentration at the outlet was measured over time (fig. 1). After a rapid increase, the CH_4 concentration at the chamber outlet decreased exponentially. The response time of the chamber towards changes in the pCH_4 was calculated as the reciprocal of the slope to be 62±8 s. Steady state is almost re-established after less than 300s. It has to be noted that the response time of the analytical system is in the same order as those of the chamber. Thus the response time of the chamber for methane may actually be shorter than calculated above.

DIC (Dissolved Inorganic Carbon)

CO2 sources or sink inside the chamber affect the carbonate equilibrium inside the chamber. Thus we have to address the entire DIC pool (DIC = sum of dissolved carbonate bicarbonate

and CO_2) to assess the carbon dynamics. The response time for DIC was determined in a similar way as the response time for the inert trace gases but with an inlet concentration being in equilibrium with the initial partial pressure of the dissolved CO_2 ($pCO_{2)}$ of the seawater solution inside the chamber.

An artificial seawater solution with35 PSU, a DIC concentration of 1960±15 µmol kg^{-1} and a carbonate and borate alkalinity of 2180±15 µeg Kg^{-1} was prepared. The pH of the solution was adjusted to 8.09±0.01 yielding a pCO_2 of 425±10 ppm at 296.5 K. The synthetic air was doped with pure CO_2 (Westfalen Germany) providing a CO_2 inlet concentration of 425±10 ppm at a flushing flow rate of 3.29 L min^{-1}. Thus the carbonate system was initially in equilibrium with the purge gas. The pH inside the chamber was measured during the CO_2 experiments with a Schott CG 841 pH meter. 250 ml of seawater were withdrawn from the chamber and were equilibrated with CO_2 (30% in synthetic air) for 3h at 1.3 bar and 23.5°C. After injection of 250ml of the DIC enriched seawater the pH rapidly dropped to 7.5 and the CO_2 concentration at the chamber outlet increased from 426 ppm to 1277 ppm within 1.5 min. Figure 2 shows the following decrease of the CO_2 outlet concentration, the DIC and the increase in pH over time. Within the first hour the CO_2 outlet concentration decreased to 439 ppm. After 1.67h (6000s) the CO_2 outlet concentration remained stable at 429.6±0.6 ppm. The CO2 flux concurrently declined from 186 mmol m^{-2} h^{-1} to zero. The ΔDIC relative to the initial conditions was recalculated from the flux and was 188±3 µmol kg^{-1} at the beginning of the experiment. Steady state conditions were almost re-established within 1.5 hrs.

After this experiment, the chamber was flushed with CO_2 free synthetic air for 2.5 hours at a flushing flow rate of 5 L min^{-1} to lower the DIC inside the chamber. The DIC inside the chamber was lowered by 210±4 µmol kg^{-1} as calculated from the CO_2 flux. Concurrently the pH increased to 8.36. Afterwards the purge flow was set to 3.29 L min^{-1} again and the CO_2 inlet concentration was readjusted to 425±10 ppm to monitor the response time for the CO_2 uptake (fig. 3). At the beginning of the experiment the outlet concentration rapidly increased from 231 to 300 ppm and then more slowly to 367 ppm within the first hour. After 2 h the outlet concentration was 419 ppm and then gradually increased to 426 ppm at the end of the experiment. The CO_2 flux followed the outlet concentration and was -28 mmol m^{-2} h^{-1} at the beginning of the experiment. 72% of the DIC were replenished after 1h and 96% (203±3 µmol kg^{-1}) were replenished after 2.4h at the end of the experiment.

In contrast to methane neither CO_2 emission nor CO_2 uptake followed an exponential trend. The reason is that the flux is determined by the concentration of the dissolved CO_2 that varies with the DIC.

The instantaneous response (t_{rwi}) time that can be estimated from the instantaneous flux F_i and the deviation of the DIC from equilibrium with the CO_2 inlet concentration (ΔDIC_i) and the chamber volume (V_k)

$$t_{rwi} = \frac{V_k \Delta DIC_i}{F_i} \quad (13)$$

The instantaneous response times were calculated from the measured and the calculated fluxes. Under the experimental conditions the instantaneous response time of the DIC in case of emission increased from 10 min. at a ΔDIC of 188 µmol kg^{-1} to 22 min. at a ΔDIC of 1 µmol kg^{-1}. In case of CO2 uptake the experimental response times increased from 27 minutes for a ΔDIC of- 5 µmol kg^{-1} to 58 min at a ΔDIC of- 195 µmol kg^{-1}. In both cases the change in the instantaneous response time is primarily governed by the ratio of dissolved CO_2 to DIC.

A simple model was used to recalculate the chamber CO_2 flux from the pCO_2. Carbonate speciation was calculated for a DIC range from 1760 to 2160 µmol kg^{-1} for a constant temperature of 296.5K and an alkalinity of 2200 µeq kg^{-1}. This calculation was made with the spreadsheet of Pierrot et al. (2006) utilizing the code of Lewis & Wallace 1998 and this data were used to prescribe the dissolved CO_2 as a function of DIC:

$$[CO_2] = a \times DIC \quad (16)$$

Thus for DIC eq. 15 becomes:

$$a_t \times DIC_{(t)} = (a_t \times DIC_{(0)} - c_{in} \times H) \times e^{-\frac{t}{V \times H \times R_{aw}}} \quad (17)$$

At a DIC of 1960 µmol kg^{-1} and a pCO_2 of 429.2 ppm the chamber was assumed to be in equilibrium with the CO_2 inlet concentration. For CO_2 emissions the best fit to the experimental data was obtained with $VxHXR_{aw}$ = 135s. For CO_2 uptake the best fit to the experimental data was obtained with $VxHXR_{aw}$ = 390s. Thus the CO_2 emission is about three times faster than the CO_2 uptake. We attribute this difference to differences in the release and uptake kinetic of CO_2. The governing reaction for the CO_2 release is the protonation of the bicarbonate, whereas the uptake is governed by the hydration of CO_2. As shown in figure 4 this simple model can sufficiently resemble the measured fluxes with $R^2 > 0.99$. This model

was used to assess the effect of water exchange and to estimate the recovery for the interfacial flux under the experimental conditions.

Effect of the water exchange

During tidal inundation the chamber is connected to the surrounding waters via U-tube at the bottom (stainless steel tube 50 cm length, 4 mm i.d.) to assure pressure equilibrium. This inevitably leads to an exchange of water between the chamber and the surrounding water body that may thus affect the flux measurements.

The flux through the U-tube depends on the pressure gradient between the chamber and the surrounding water and is thus mainly modulated by wave actions. The flux measurements were carried out under calm conditions with wind speeds rarely exceeding 5 ms^{-1} and wave heights below 10 cm. For a pressure difference of 1 kPa is the measured flow 308±7 ml min^{-1}. This is about 46% of the theoretical flow expected from Hagen-Poiseilles law reflecting the narrowing of the tube at the bendings. The wave induced pressure oscillations cause an oscillating flow between the chamber and the surrounding water body. When assuming sinusoidal waves with amplitude of 5cm the water exchange rate is 46 ml min^{-1} resulting in a water exchange resistance of 130 min being substantially larger than the respective response times for the gas exchange. In our study the flux was computed from the difference between the inlet and outlet concentration neglecting the effect of the water exchange and the change of the concentration inside the chamber. The resulting bias can be estimated from eq. 10. Therefore we i) assume a constant trace gas flux into the chamber and ii) the surrounding water being always in equilibrium with the atmosphere. The resulting bias is -0.3% for CH_4. Thus we can safely assume that the bias due to water exchange is negligible for CH_4.

Due to the much slower response of the carbonate system the bias becomes larger for DIC. Table 1 shows the the recovery of the true interfacial flux at the chamber outlet for constant fluxes ranging from -30 to 30 mmol m^{-2} h^{-1} and an incubation time of 6 h. Without any water exchange the DIC recovery ranges from 86% at -30 mmol m^{-2} h^{-1} to 94.5% at30 mmol m^{-2} h^{-1}. When including the water exchange the recovery ranges from 68% at-30 mmol m^{-2} h^{-1} to 84% at 30 mmol m^{-2} h^{-1}. Benthic respiration and assimilation will shift DIC pools inside and outside of the chamber into the same direction. Due to the enclosure effect the shift is more pronounced inside the chamber. This may to some extent reduce the effect of the water exchange. However, we found this recovery acceptable for a first tentative assessment of the DIC dynamics over full tidal cycles as was the primary goal of our study. An accurate

determination of carbon fluxes in future studies require additional measures such as pH or alkalinity to better constrain the carbonate system. Further the water exchange between the chamber and surrounding waters should be quantified. The performance of the chamber under submersed can be improved by reducing the response time. This can be achieved by reducing the chamber volume or increasing the air flow through the chamber.

Tables

Table 1: Simulated fluxes and recovery rates for interfacial fluxes ranging from -30 to 30 mmol $m^{-2}h^{-1}$. F_i denotes the true interfacial flux, F_{out} is the flux at the chamber outlet and F_w is the flux through the U-tube. Fw has been computed against a DIC concentration of 1960 µmol kg^{-1} outside the chamber being in equilibrium with the air. DIC (6h) provides the DIC concentration after 6h of incubation and the recovery is given by the ratio of F_{out} to F_i.

F_i mmol $m^{-2}h^{-1}$	**F_{out} mmol $m^{-2}h^{-1}$**	**F_w mol $m^{-2}h^{-1}$**	**DIC(6h) µmol kg^{-1}**	**Recovery Fout/Fi**
-30	-22.4	7.5	1844	0.68
-20	-15.4	4.5	1890	0.71
-15	-11.7	3.2	1910	0.72
-10	-7.9	2.1	1929	0.73
-5	-3.9	1.0	1945	0.74
5	4.2	-0.7	1971	0.81
10	8.6	-1.3	1981	0.82
15	13.0	-1.9	1990	0.83
20	17.4	-2.5	1999	0.83
30	26.3	-3.6	2015	0.84

Figures

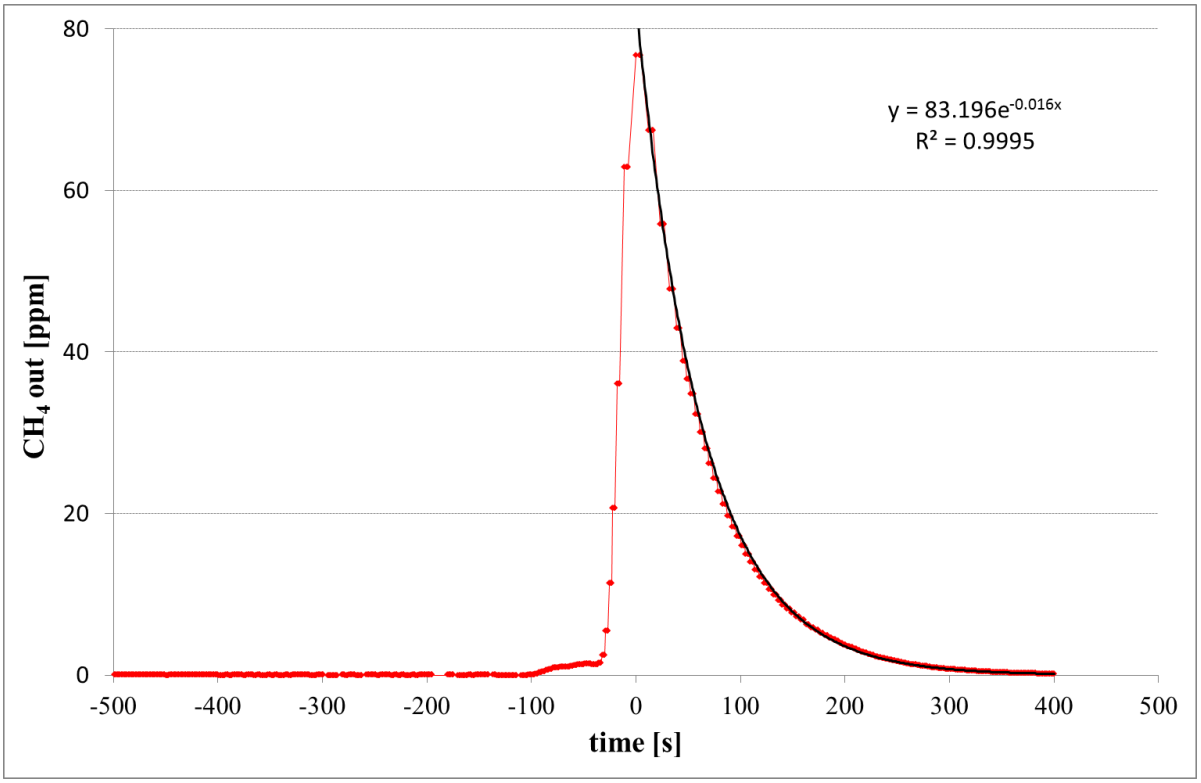

Figure 1: Evolution of CH_4 concentration at the chamber outlet after injection of 250 ml of seawater containing 14.3 µmol CH_4. The regression is calculated for the decrease in the CH_4 concentration.

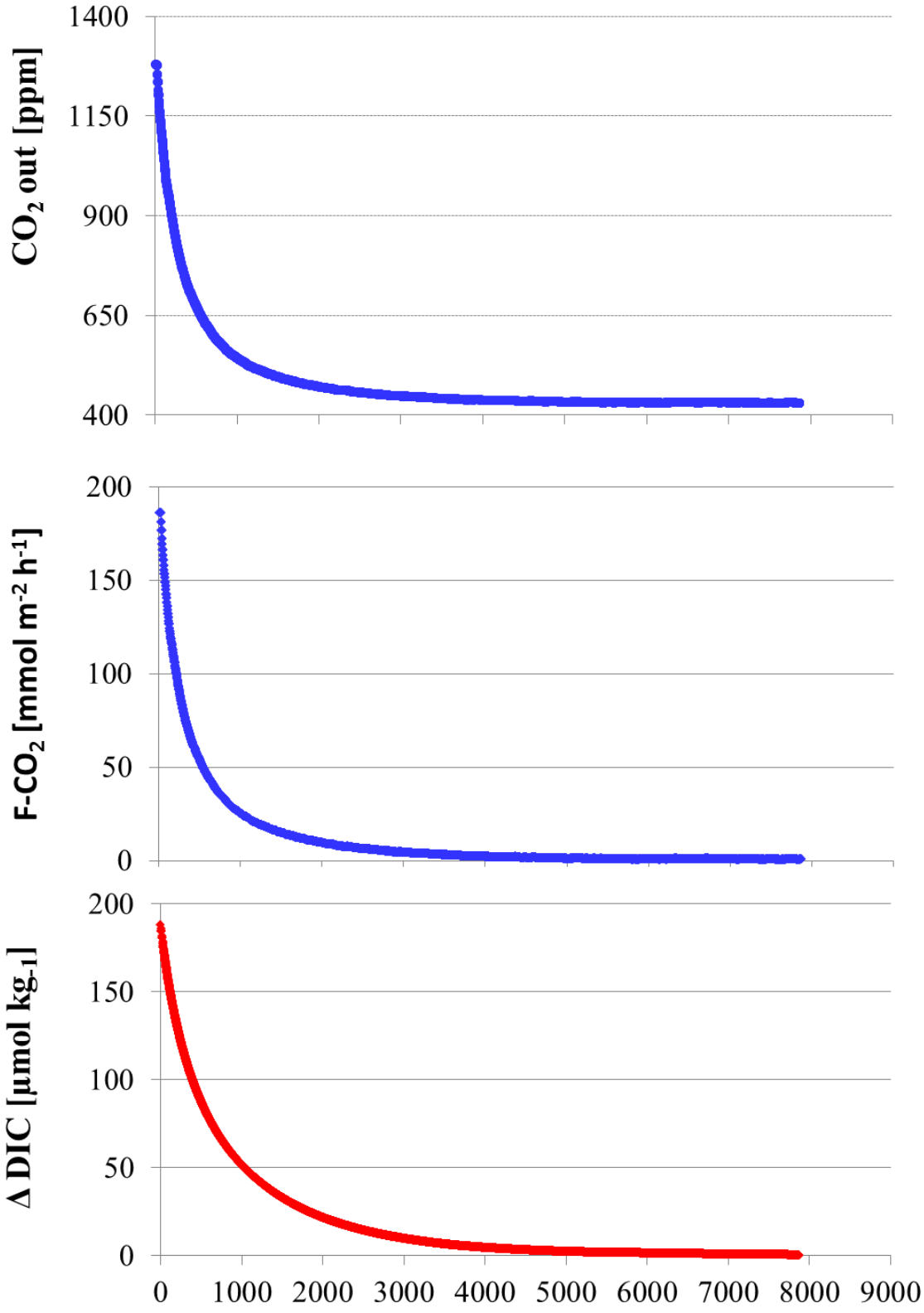

Figure 2: Evolution of CO_2 outlet concentration, flux and ΔDIC after increasing the DIC from 1960 to 2148 µmol kg^{-1} at an alkalinity of 2200 µeq kg^{-1}. The change in DIC has been calculated from the CO_2 flux. The CO2 inlet mixing ratio was 425±10 ppm.

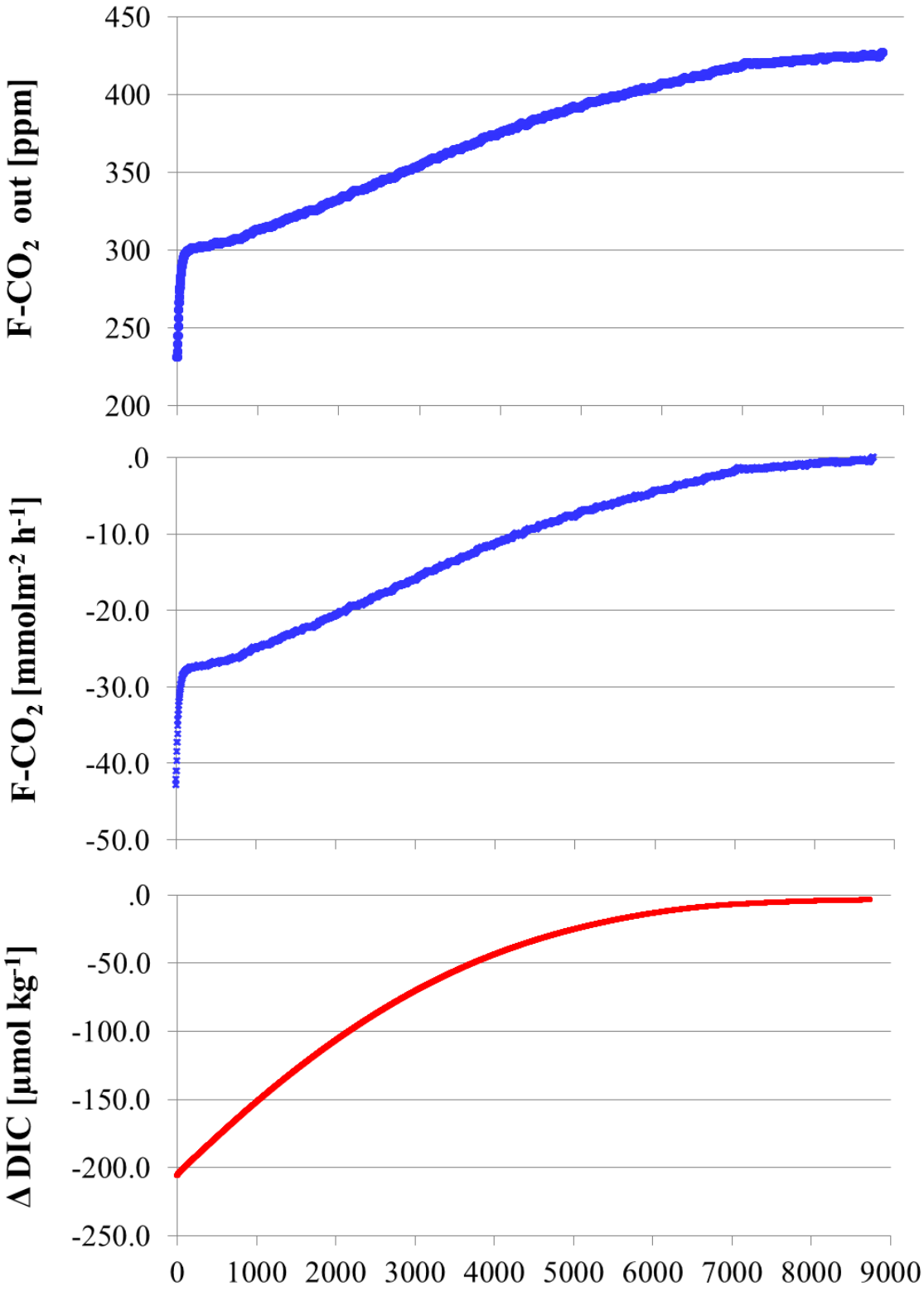

Figure 3: Evolution of CO_2 outlet concentration, flux and ΔDIC after lowering the DIC from 1960 to 1757 µmol kg^{-1} at an alkalinity of 2200 µeq kg^{-1}. The change in DIC has been calculated from the CO_2 flux. The CO2 inlet mixing ratio was 425±10 ppm.

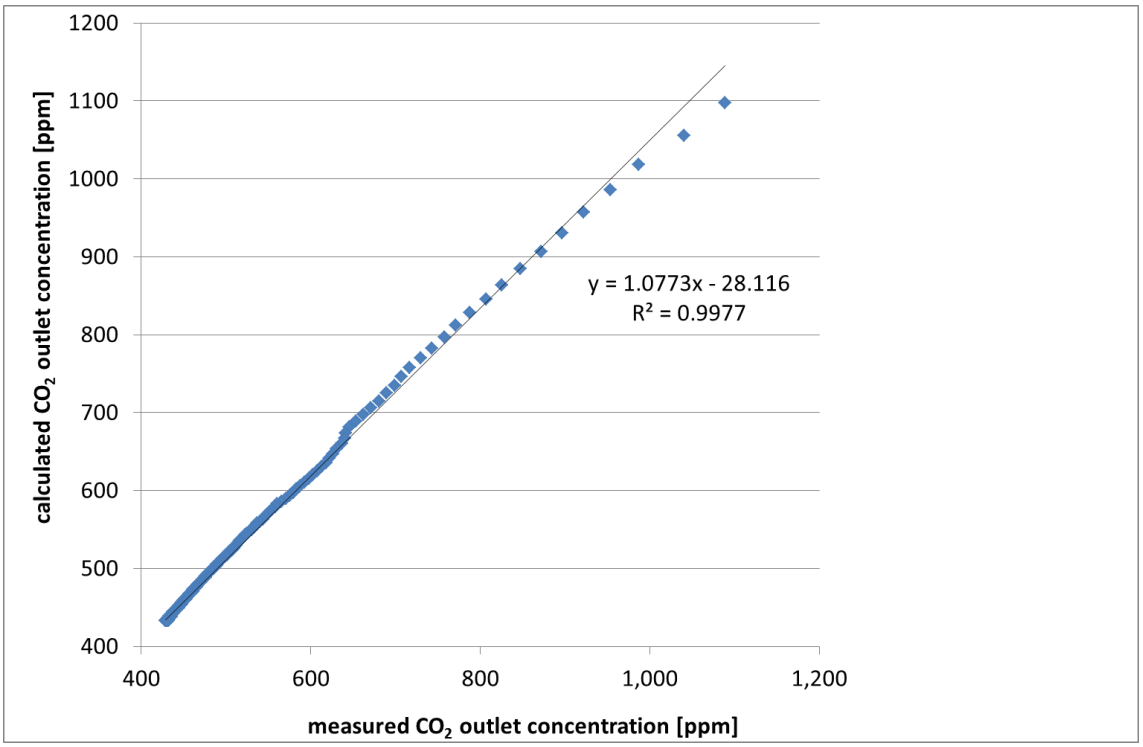

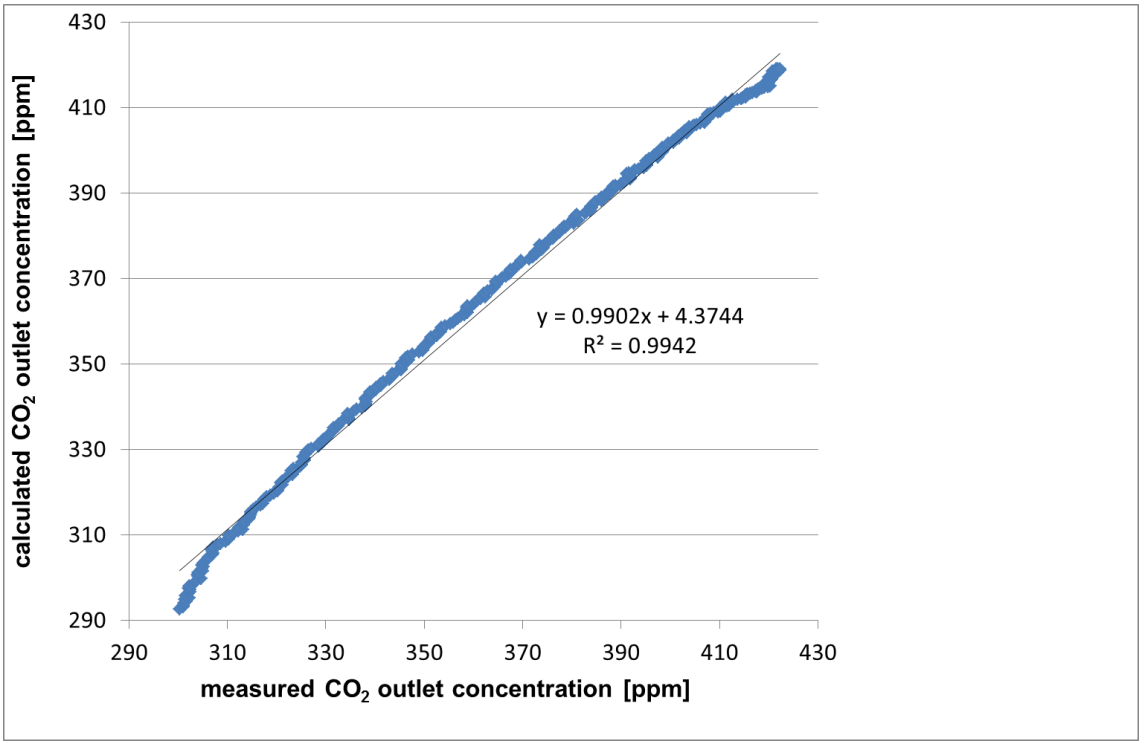

Figure 4: Comparison of the measured and calculated CO_2 outlet mixing ratios for emissions (upper panel and uptake (lower panel.

References

Billerbeck, M., Werner, U., Bosselmann, K., Walpersdorf, E., Huettel, M., 2006a. Nutrient release from an exposed intertidal sand flat. Marine Ecology Progress Series 316, 35-51.

Cook, P.L.M., Wenzhöfer, F., Glud, R.N., Jansen, F., Huettel, M. 2007. Benthic solute exchange and carbon mineralization in two shallow subtidal sandy sediments: Effect of advective pore-water exchange. Limnology and Oceanography 52, 1943 - 1963

Gao, F., Yates, S.R., Yates, M.V., Gan, J.Y., Ernst, F.F., 1997. Design, fabrication, and application of a dynamic chamber for measuring gas emissions from soil. Environmental Science & Technology 31, 148-153.

Gao, F., and Yates, S. R.: Laboratory study of closed and dynamic flux chambers: Experimental results and implications for field application, J. Geophys. Res.-Atmos., 103, 26 115–26 125, 1998.

Hicks, B. B., Baldocchi, D. D., Meyers, T. P., Hosker, R. P., and Matt, D. R.: A Preliminary Multiple Resistance Routine for Deriving Dry Deposition Velocities from Measured Quantities, Water Air and Soil Pollution, 36, 311–330, 1987

.Huettel, M., Ziebis, W., Forster, S., 1996. Flow-induced uptake of particulate matter in permeable sediments. Limnology and Oceanography 41, 309-322.

Jansen, S., E. Walpersdorf, U. Werner, M. Billerbeck, M.E. Böttcher and D. de Beer (2009). Functioning of intertidal flats inferred from temporal and spatial dynamics of O2, H2S and pH in their surface sediment. Ocean Dynamics 59, 317-332.

Kim, K.H., Lindberg, S.E. (1995): *Design and initial tests of a dynamic enclosure chamber for measurements of vapour phase mercury fluxes over soils,* Water, Air and Soil Pollution, 80, 1059-1068

Lewis, E., and D. W. R. Wallace. 1998. Program Developed for CO2 System Calculations. ORNL/CDIAC-105. Carbon Dioxide Information Analysis Center, Oak Ridge National Laboratory, U.S. Department of Energy, Oak Ridge, Tennessee

Meixner, F.X., Fickinger, T., Marufu, L., Serca, D., Nathaus, F.J., Makina, E., Mukurumbira, L., Andreae, M.O., 1997. Preliminary results on nitric oxide emission from a southern African savanna ecosystem. Nutrient Cycling in Agroecosystems 48, 123-138.

Pape, L., Ammann, C., Nyfeler-Brunner, A., Spirig, C., Hens, K., Meixner, F.X., 2009. An automated dynamic chamber system for surface exchange measurement of non-reactive and reactive trace gases of grassland ecosystems. Biogeosciences 6, 405-429.

Penman, H.L. 1940a. Gas and vapor movements in the soil. I. The diffusion of vapors through porous solids, *J. Agr. Sci.*, 30:437–462.

Penman, H.L. 1940b. Gas and vapor movements in the soil. II. The diffusion of carbon dioxide through porous solids, *J. Agr. Sci.*, 30:570–581.

MacFarlane J.J 1992 Perm Permeability of the cuticle of Vallisneria spiralis to carbon dioxide and oxygen, Aquatic Botany 43: 129-135

Pérez-Lloréns JL, Niell FX (1993) Seasonal dynamics of biomass and nutrient content in the intertidal seagrass *Zostera noltii* Hornem. from the Palmones river estuary, Spain. Aquat Bot 46:49–66

Pierrot, D. E. Lewis,and D. W. R. Wallace. 2006. MS Excel Program Developed for CO2 System Calculations. ORNL/CDIAC-105a. Carbon Dioxide Information Analysis Center, Oak Ridge National Laboratory, U.S. Department of Energy, Oak Ridge, Tennessee. doi: 10.3334/CDIAC/otg.CO2SYS_XLS_CDIAC105a

Tengberg, A., Stahl H., G. Gust, G., V. Mueller, V., U. Arning, U., Andersson, H., Hall, P.A.J., 2004. Intercalibration of benthic flux chambers I. Accuracy of flux measurements and influence of chamber hydrodynamics. Progress in Oceanography 60 (2004) 1–28

Werner, U., Billerbeck, M., Polerecky, L., Franke, U., Huettel, M., van Beusekom, J.E.E., de Beer, D., 2006. Spatial and temporal patterns of mineralization rates and oxygen distribution in a permeable intertidal sand flat (Sylt, Germany). Limnology and Oceanography 51, 2549-2563.

Zhang, H., Lindberg, S.E., Barnett, M.O., Vette, A.F., Gustin, M.S., 2002. Dynamic flux chamber measurement of gaseous mercury emission fluxes over soils. Part 1: simulation of gaseous mercury emissions from soils using a two-resistance exchange interface model. Atmospheric Environment 36, 835-846.